Heliyon 10 (2024) e25919

Contents lists available at ScienceDirect

Heliyon

journal homepage: www.cell.com/heliyon

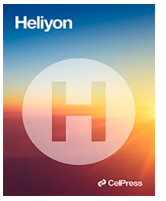

Research article

# Application of montmorillonite/octadecylamine nanoparticles in the removal of textile dye from aqueous solutions: Modeling, kinetic, and equilibrium studies

Fatemeh Keshavarzi [a], Mohammad Reza Samaei [b,*], Hassan Hashemi [b], Abooalfazl Azhdarpoor [b], Amin Mohammadpour [a]

[a] Department of Environmental Health Engineering, School of Public Health, Student Research Committee, Shiraz University of Medical Sciences, Shiraz, Iran
[b] Department of Environmental Health Engineering, School of Public Health, Shiraz University of Medical Sciences, Shiraz, Iran

ARTICLE INFO

*Keywords:*
Textile wastewater
Dye
Ultrasonic
Nanoclay modified with octadecylamine
Adsorption

ABSTRACT

In the study, the proliferation of industries has been associated with an increase in the production of industrial wastewater and subsequent environmental pollution, wherein dyes emerge as prominent pollutants. The characteristics of nanoclay modified with octadecylamine, were elucidated throughvarious techniques, including Field Emission Scanning Electron Microscopy/Energy Dispersive Spectroscopy (FE-SEM/EDS), Fourier Transform Infrared Spectroscopy (FTIR), Thermogravimetric Analysis (TGA), X-ray Diffraction (XRD), and Brunauer-Emmett-Teller Surface Area Analysis (BET). The research delved into the impact of variables such as pH, initial dye concentration, adsorbent dose, temperature, and ultrasonication time on the removal of Acid Black 1 (AB1) through an ultrasonic process, employing a central composite design (CCD). Optimal conditions for the adsorption process were determined: pH at 5.46, adsorbent mass at 4 mg/30 mL, initial dye concentration at 20 mg/L, ultrasound time at 20 min, and temperature at 50 °C, resulting in a remarkable 96.49% adsorption efficiency. The fitting of experimental equilibrium data to different isotherm models, including Langmuir, Freundlich, and Temkin, indicated thatthe Freundlich model was the most suitable. Analysis of the adsorption data with various kinetic models such as pseudo-first and second-order models, and intraparticle diffusion models, revealed the applicability of the second-order equation model. A thermodynamic study unveiled that the adsorption process was spontaneous and endothermic. In conclusion, the study highlights the significant capability ofmontmorillonite nanoclay modified with octadecylamine in removing AB1 dye, rendering it a viable option for wastewater treatment.

## 1. Introduction

In recent years, the rapid expansion of industrial activities has led to a significant increase in the generation of industrial wastewater, resulting in heightened environmental pollution [1–3]. Among the various contaminants, dyes stand out as particularly crucial contributors to industrial wastewater pollution [4,5]. The discharge of dyed wastewater, especially from industries such as textiles, not

* Corresponding author
*E-mail addresses:* mrsamaei@gmail.com, mrsamaei@sums.ac.ir (M.R. Samaei).

https://doi.org/10.1016/j.heliyon.2024.e25919
Received 21 March 2023; Received in revised form 2 February 2024; Accepted 5 February 2024
Available online 10 February 2024

only adversely affects the aesthetic appeal of receiving waters but also hinders essential photosynthesis processes [6,7]. Notably, the textile industry emerges as a primary source of dye effluent, contributing for more than half (54%) of the total dye pollution in the environment. Other notable contributors to dyed waste encompass the dyeing industry (21%), the paper and pulp industry (10%), the tannery and paint industry (8%), and the paint production industry (7%). Predominantly, the dyes employed in these industries are synthetic [8,9]. Synthetic dyes, commonly classified into categories such as acid dyes, reactive dyes, direct dyes, basic dyes, and other groups, constitute the majority of the coloring agents utilized [10]. Most dyes are characterized by the presence of one or more benzene rings, known fortheir toxicity and slow degradation, posing a substantial risk of environmental harmif released untreated [11]. Consequently, it becomes imperative to implement effective waste treatment measures before discharging such pollutants into the environment.

To date, various methods, including biological processes, membrane technologies, and advanced oxidation processes, have been employed in the treatment ofthis particular type of wastewater [12–15]. Among these methods, the surface adsorption process stands out as one of the most prevalent techniques in water and wastewater treatment. Typically, activated carbon is the material of choice for surface adsorption processes. However, commercial activated carbon is often characterized by high costs and demands expertise for its application. Moreover, the reuse of commercial activated carbon necessitates regeneration, imposing constraints on its widespread utilization [16]. Given these challenges, researchers are increasingly exploring alternatives to commercial activated carbon for the removal of organic pollutants. The use of natural and cost-effective adsorbents has emerged as a notable focus in research endeavors.

Nanoparticles, characterized by dimensions spanning a sub-micrometer scale from 1 to 100 nm, exhibit unique physicochemical attributes influenced by their diminutive size and elevated surface-to-volume ratio [17]. These nanoparticles exhibit significantdeviation in behavior compared to their bulk material counterparts [18]. Their heightened reactivity and increased surface area render them particularly effective in e various nvironmental applications, including the removal of pollutants for the enhancement of water and air quality enhancement [19–21]. Montmorillonite (MMT), a nano-clay particle that constitutes that constitutes the principal phase in bentonite, boasts dimensions of approximately 10 Å. This nano-clay exhibits distinctive characteristics, including swelling in polar environments, a high specific surface area, surface electrical properties, and cation exchange capacity, rendering it a material of considerable interest [22]. Owing to its notable attributes such as high-water absorption potential and negative surface charge, facilitated by ion exchange, Montmorillonite has the capability to absorb various organic cations, including pesticides, dyes, surfactants, phenols and detergents. Montmorillonite demonstrates the capability to absorb not only inorganic substances such as pesticides and dyes but also inorganic substances including heavy metals like Ni, Cu, Ag, Co. Its performance surpasses that of other reference clay soils, including quartz, calcium carbonate, kaolin and illite. In water purification processes, various methods have been employed to modify and functionalize the surface of nanoclays [23,24]. Surface modification enhances the performance of nanoclays by increasing the distance between clay layers, creating new absorption sites, and improving porosity, thereby augmenting their absorption capacity [25].

Octadecylamine, a modifier with the formula C18H39 N is classified as a powerful base compound based on its pKa. It comprises a hydrophilic amine group and a hydrophobic alkyl group [26]. This modifying group, characterized by the hydrophobic carbon chain connected to the central atom, forms a bond with the MMT nanoclay layers. This interaction increases the distance between nanoclay layers and expands the surface of these nanoparticles. Azo-type dyes, characterized by an azo group consisting of two nitrogen atoms (–N=N–) represent the largest category of dyes, constituting over half of the global dye production [27]. The AB1dye, belonging to this class, is an anionic azo dye with a molecular weight of 616.49 g/mol and a a chemical formula of C22H16N60O9S22Na, with a mass of 618.54 g/mol. High concentrations of acid black 1 in wastewater pose significant health risks, including respiratory problems, skin irritation, and eye discomfort [28,29].

This scholarly investigation elaborates on the creation and comprehensive characterization of a montmorillonite clay nanoadsorbent, functionally enhanced with an octadecylamine group. The primary objective of this development is to enhance the efficacy of AB1 dye removal, a prevalent contaminant in the textile sector, facilitated through an ultrasound process. The study meticulously examines critical factors, including the adsorbent dose, initial dye concentration, temperature, contact duration, and pH, to unravel the intricacies of this innovative system.

Furthermore, the CCD technique is employed to optimize experimental conditions, thereby enhancing the efficiency of AB1 dye removal and consequently mitigating its associated environmental risks. Finally, The investigation encompasses the application of isotherm, kinetic, and thermodynamic adsorption models, providing a comprehensive analysis of the complexities inherent in the AB1 dye removal procedure. The scientific novelty of this study lies in its integrated approach to materials design, process analysis, and optimization, with potential implications for develo development of ping more efficient and eco-friendly pollutant removal methods in the textile industry.

## 2. Materials and methods

### *2.1. Materials*

The azo dye AB1, boasting a purity of 99%, was procured from Elvan Thabit, Iran. Hydrochloric acid (concentration 37%) and sodium hydroxide (purity >99%) were sourced from Merck, Germany. Additionally, octadecylamine (purity >99%) and montmorillonite nanoclay (K10) were acquired from Sigma-Aldrich, in the USA. All chemicals used were of laboratory grade and were employed as received, without necessitating furtherpurification. The preparation of all necessary reagents and solutions was conducted using double distilled water, to ensure high purity and maintain consistency in the experimental conditions.

### 2.2. Preparation of stock solution

A stock solution of AB 1 dye, with a concentration of 1000 mg/L, was prepared by dissolving 1 g of the dye in 1000 mL of deionized water. To create standard solutions for experimental tests, appropriate dilutions were performed using the prepared stock solution. The pH of these solutions was meticulously regulated using standard concentrations of hydrochloric acid and sodium hydroxide.

### 2.3. Nanoclay synthesis and modification process

The surface functionalization of MMT nanoclay was conducted as follows: Initially, 5 g of MMT nanoclay adsorbent was dispersed in 500 mL of deionized water and agitated at room temperature for 24 h using a magnetic stirrer. Subsequently, 2 g of octadecylamine were dissolved in 60 mL of ethanol, and this solution was gradually introduced into the MMT nanoclay dispersion, serving as a modification agent.Following a reaction period of 12 h, during which the octadecylamine interacted with the MMT nanoclay particles, the resulting modified nanoclay was separated from the mixture via filtration using filter paper. The collected solid residue underwent heat treatment at 100 °C for a 4 h to ensure the complete evaporation of residual moisture from the composition.

### 2.4. Measurement of adsorption

To quantify the degree of dye removal, sampling was conducted at various intervals of contact time. The extent of dye adsorption was subsequently assessed through a spectrophotometric procedure at a wavelength of 622 nm. The residual dye concentration was determined by referencing a previously prepared calibration curve. Sampling for each variable parameter was carried out on three separate occasions, and the mean value of these measurements was considered for subsequent calculations. The percentage removal of the dye was calculated using equation (1):

$$Removal\ (\%) = \frac{(C_0 - C_e) \times 100}{C_0} \tag{1}$$

$C_0$ = initial concentration of dye.
$C_e$ = final concentration of dye.

### 2.5. Experiment design

In this investigation, we employed the Response Surface Methodology (RSM) centered on the Central Composite Design for optimization and evaluation of the influence of independent variables, as well as the combined interaction between these variables, on the response performance (efficiency of AB1 dye removal). This was carried out using Design-Expert software (Version 13.0.0). The proposed software model underwent analysis via Analysis of Variance (ANOVA), and the model's effectiveness was evaluated using R-squared (R2) and adjusted R-squared values. Parameters influencing the study, including contact time, pH, initial dye concentration, temperature, and adsorbent dose were systematically evaluated in discrete phases throughout the research. The respective values of these parameters are documented in Table 1.

### 2.6. Kinetic and isotherm studies

In the present investigation, we evaluated the adsorption kinetics of the AB1 dye using montmorillonite nanoclay modified with octadecylamine. The primary objective was to comprehend the behaviour of this particular adsorbent. To achieve this, three different models were deployed: the pseudo-first-order, pseudo-second-order, and intraparticle diffusion models. The corresponding equations for these three models are presented as Equations (2)–(4) [30]:

$$log(q_e - q_t) = log\ q_e - \frac{k_1 t}{2.3} \tag{2}$$

$$\frac{t}{q_t} = \frac{1}{k^2\ q_e^2} + \left(\frac{1}{q_e}\right) t \tag{3}$$

**Table 1**
Parameters and design levels of AB1 removal test.

| – | Parameter | Unit | Code | | | | |
|---|---|---|---|---|---|---|---|
| | | | -2α | -α | 0 | α | +2α |
| 1 | Time | (min) | 6.22 | 20 | 30 | 40 | 53.58 |
| 2 | Initial concentration | (mg/L) | 6.22 | 20 | 30 | 40 | 53.78 |
| 3 | Absorbent dose | (mg/30 mL) | 0.62 | 2 | 3 | 4 | 5.38 |
| 4 | Temperature | (°C) | 16.21 | 30 | 40 | 50 | 63.78 |
| 5 | pH | (–) | 3.24 | 5 | 7 | 9 | 11.75 |

$$q_t = K_p t^{0.5} + C \tag{4}$$

Adsorption isotherms are mathematical models employed to illustrate the equilibrium state between the adsorbate portions in both the solid and liquid phases. In the context of this study, data derived from adsorption equilibrium experiments were comprehensively examined utilizing three prominent isotherm models: Freundlich, Langmuir, and Temkin. The Langmuir isotherm, in particular, establishes a nonlinear relationship, which is represented in the form of Equation (5) [31]:

$$q_e = \frac{q_m b C_e}{1 + bC_e} \tag{5}$$

The nonlinear form of the Langmuir equation can be transformed into equation (6) By integrating the above relation:

$$\frac{C_e}{q_e} = \frac{1}{bq_m} + \frac{C_e}{q_m} \tag{6}$$

In this context, qe represents the amount of adsorbed component per unit mass of the adsorbent body (mg/g), Ce denotes the equilibrium concentration of the adsorbable substance in the solution after surface adsorption (mg/l), qm indicates the maximum adsorption capacity, and b is the Langmuir constant. These parameters are obtained by plotting Ce/qe versus Ce. The separation factor (RL) is a crucial parameter that gauges the effectiveness of the adsorption mechanism by establishing the relationship between the adsorbent and the adsorbate. It is calculated using equation (7):

$$R_L = \frac{1}{1 + bC_0} \tag{7}$$

The nonlinear equation of the Freundlich adsorption isotherm is as equation (8):

$$q_e = K_F C_e^{\frac{1}{n}} \tag{8}$$

Equation (9) represents the linear form obtained by integrating the aforementioned relationship:

$$log\ q_e = log\ K_F + \frac{1}{n} log\ C_e \tag{9}$$

In this context, Ce represents the equilibrium concentration of the absorbable substance in the solution after surface adsorption in mg/L, qe is the adsorption capacity at the equilibrium time in mg/g, and KF and n are the Freundlich constants. Temkin's isotherm equation is another equation used for hydrogen adsorption of materials on the adsorbent surface. Equation (10) shows the nonlinear form of Temkin's equation:

$$q_e = \frac{RT}{b_1} \ln(K_T C_e) \tag{10}$$

Integrating equation (10) yields the linear form of Temkin's equation, represented as equation (11):

$$q_e = B_1 \ln(K_T) + B_1 \ln(C_e) \tag{11}$$

In this relation, where B1 = RT/b1, b1 represents the adsorption temperature, and KT represents the maximum adsorption energy.

The type of adsorption can be determined by thermodynamic quantities such as Gibbs free energy (ΔG), entropy change (ΔS) and enthalpy change (ΔH). Thermodynamic considerations of an adsorption process are necessary to conclude whether the process is spontaneous or not. The ΔG is calculated using Equations (12)–(14):

$$\Delta G = -RT\ Ln\ K \tag{12}$$

$$K = \frac{q_e}{Ce} \tag{13}$$

K represents the adsorption equilibrium constant (from the Langmuir model). The relationship between K and thermodynamic parameters ΔH and ΔS can be expressed by the following Van't Hoff correlation:

$$Ln\ K = \frac{\Delta S}{R} - \frac{\Delta H}{RT} \tag{14}$$

### 2.7. Characteristics of synthesized nanoclay

They investigated the surface properties, shape, constituent elements, size, and arrangement of particles on the surface of MMT nanoclay modified with octadecylamine using a scanning electron microscope (FE-SEM/EDS). The structure of the modified nanoparticles was identified using an X-ray diffraction pattern device (XRD). Additionally, the functional groups in the modified nanoclay structure were investigated using Fourier transform infrared spectroscopy (FTIR). Porosity and pore size were analyzed by BET porosity methods. Furthermore, the nanoparticles' purity evaluation and determination of thermal properties were conducted through thermal analysis.

## 3. Results and discussion

### 3.1. Characteristics of modified montmorillonite nanoclay

#### 3.1.1. XRD

Nanoclays, owing to their small size and unique crystal structure, manifest distinct diffraction patterns when exposed to X-rays, which can be effectively analyzed through XRD [32]. The XRD pattern exhibits six pronounced peaks situated at angles 20.92, 26.66, 35.12, 50.28, 62.16, and 68.28, corresponding to the (200), (110), (101), (210), (002), and (301) reflections, respectively (Fig. 1a). These peaks are indicative of the hexagonal symmetry inherent in montmorillonite nanoclay, corroborating previous studies conducted on similar materials [33–35]. Noteworthy is the absence of the (001) reflection in our analysis, a common feature in montmorillonite XRD patterns. This absence suggests that the surface modification of the nanoclay with octadecylamine has induced a contraction in the clay's interlayer spacing [36], a fascinating outcome with implications for enhanced material properties and applications. This can be attributed to the intercalation of the organic molecule within the clay layers. Employing the Scherrer equation, a widely recognized method for determining crystallite size from X-ray diffraction (XRD) patterns, we calculated the average size of the crystalline domains within the nanoparticle sample [37]. This analysis, involving the measurement of the diffraction peaks' breadth and the application of the Scherrer formula, resulted in an average crystallite size of 22.3 nm.

#### 3.1.2. FTIR

Fig. 1b depicts the infrared spectrum of modified montmorillonite, revealing distinct characteristic absorption bands. Specifically, a broad absorption band observed at the oscillation frequency of 1033.85 cm-1 can be attributed to Si–O stretching bonds. Vibrations of Me–O bonds (where Me represents a metal) are observed at a frequency fof 1466.77 cm-1 [38]. In the frequency region of 13390.86 cm-1, prominent peaks in the IR spectrum indicate the presence of limited symmetric OH stretching within the montmorillonite structure. Vibrations at 11469.76 cm-1 are distinctive of scissoring CH2 bonds. The peak at 1624.06 cm-1 corresponds to H–*O*–H bending, attributed to both Si–OH groups of mineral molecules and water in the interlayer space of montmorillonite [39]. Additionally, peaks at the frequencies of 13622.32 cm-1 are associated with structural OH stretching groups. Vibrations at 12850.19 cm-1 and

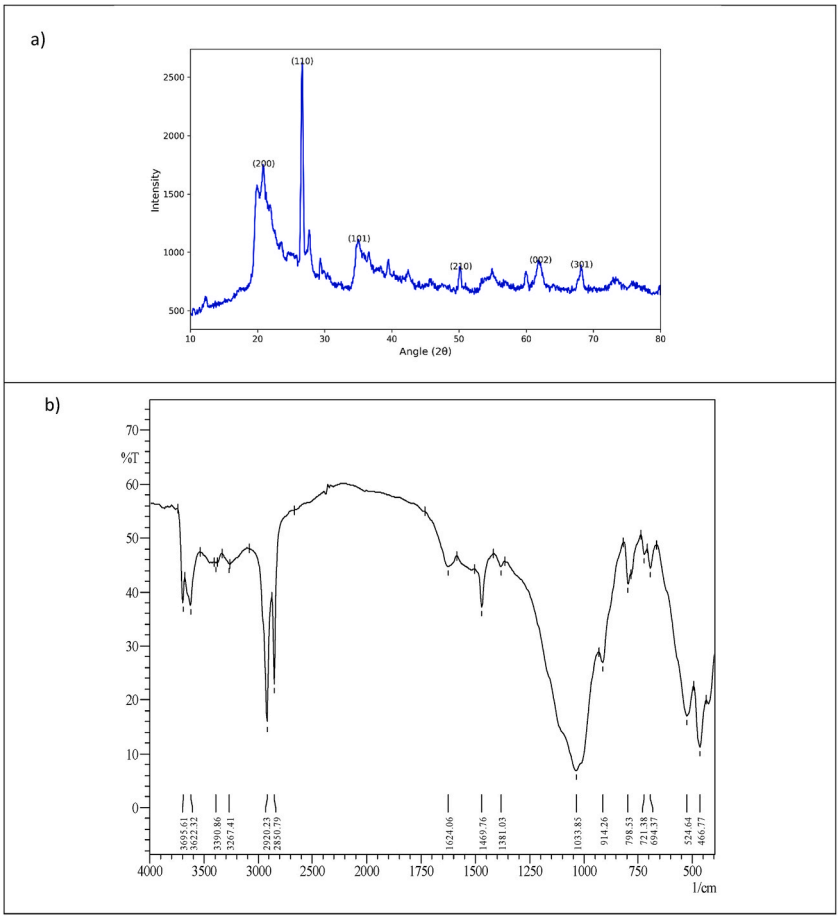


**Fig. 1.** Characteristics of montmorillonite nanoclay modified with octadecyl a)XRD, b)FTIR, c)SEM, d) EDS, e)TGA, and f) BET.

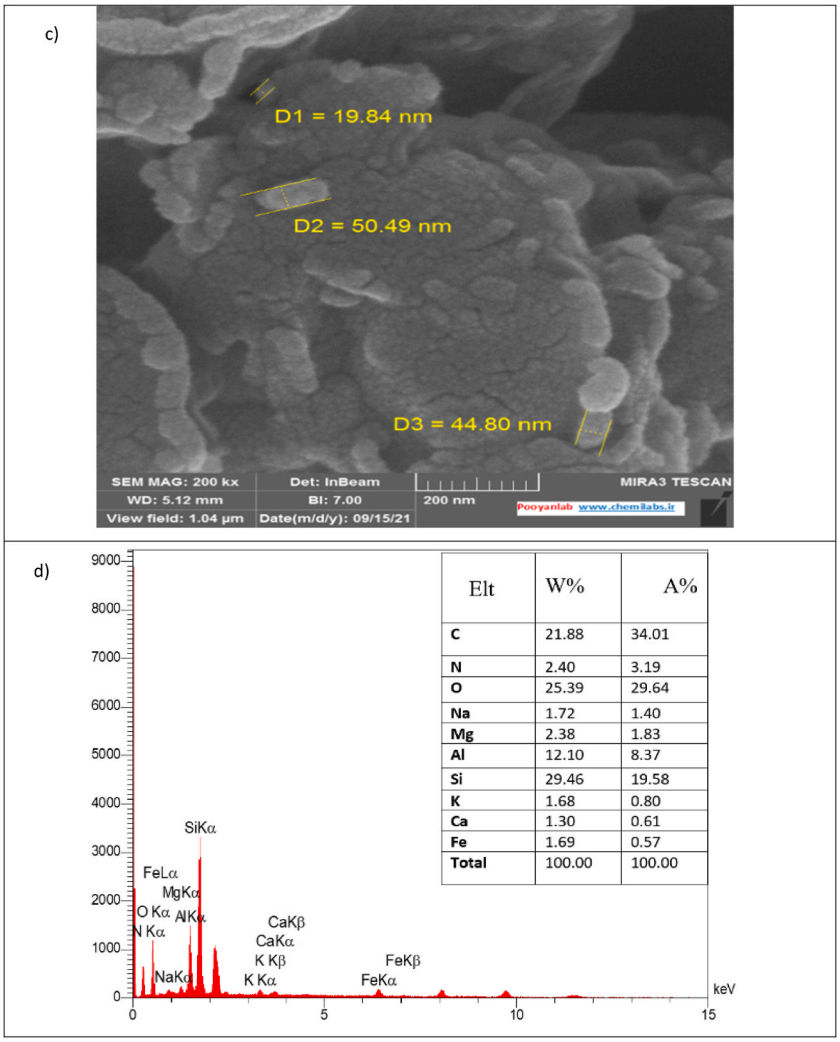


**Fig. 1.** (*continued*).

2920.23 cm-1 are attributed to the stretching vibrations of CH bonds in the -CH3 and -CH2 groups of ODA [40]. Collectively, these observations provide compelling evidence for the presence of ODA molecules in the clay structure.

### *3.1.3. FE-SEM/EDS*

Fig. 2c illustrates the FE-SEM image of montmorillonite synthesized with octadecylamine, exhibiting particles of varying sizes. The FE-SEM images reveal a regular and ordered structure with relatively uniform size. Furthermore, the octadecylamine-modified montmorillonite exhibits a hexagonal structure, and the polymerized agglomerates within this structure also display hexagonal symmetry. The particle diameters range from 19.84 nm to 50.49 nm, as depicted in the figure. Elemental composition analysis using energy dispersive X-ray spectroscopy (EDS) identified the presence of Si, O, C, Al, N, Mg, Na, Fe, and K in the modified MMT layers (Fig. 1d), with a uniform distribution of constituent elements observed.

### *3.1.4. TGA*

Thermogravimetric analysis was conducted in an artificial air environment within the temperature range of 50–800 °C (Fig. 1e). The initial degradation of montmorillonite occurred at 221.3 °C, accompanied by a weight loss of approximately 13% between 221 and 350 °C. This loss can be attributed to the desorption of water adsorbed on the octadecylamine surface, as well as the decomposition of low molecular weight species or dense side products in Si–OH groups [41]. Subsequent thermal decomposition in the range of 350–491 °C accounted for approximately 15% and is associated with the low decomposition of volatile units within the modified structure.

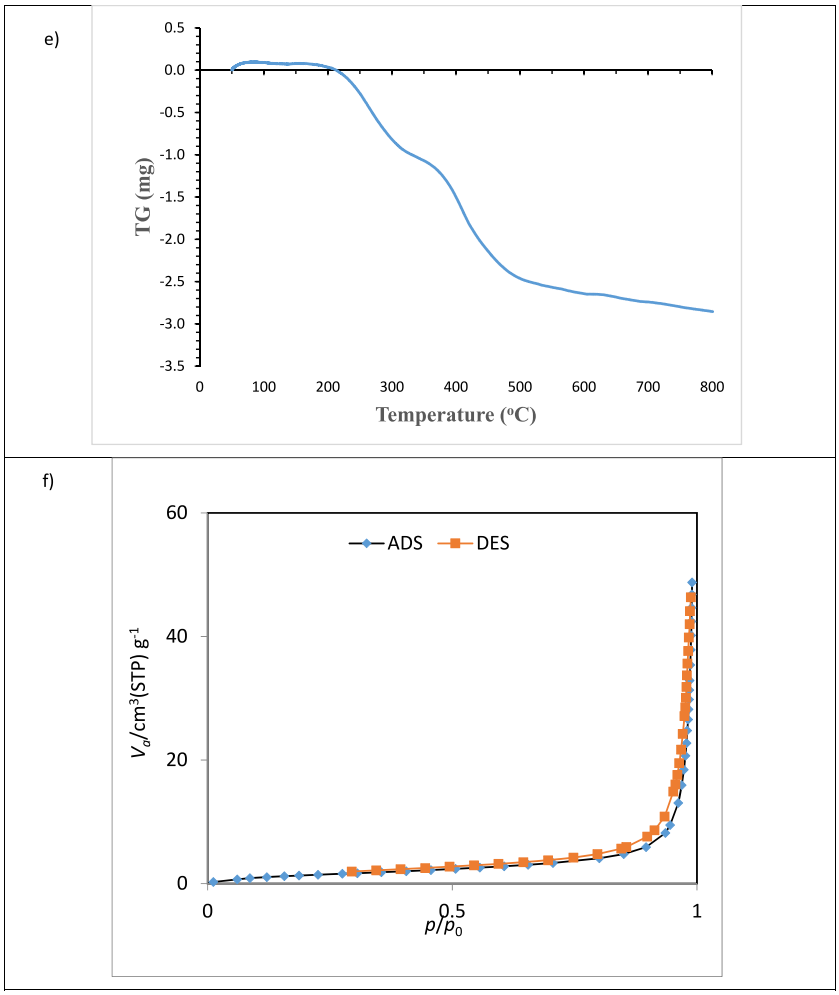


**Fig. 1.** (*continued*).

### 3.1.5. BET

The specific surface area and pore volume of the modified nanoclay were determined as 5.72 m2/g and 0.075 cm3/g, respectively. The N2 adsorption/desorption isotherms of the modified montmorillonite are displayed in Fig. 1f. According to IUPAC classification, the hysteresis loop of the adsorption isotherm falls into the H5 category, representing a relatively rare type of hysteresis loop. This classification method facilitates the categorization of pore size and morphology based on the shape characteristics of the loops. The hysteresis loop of the modified nanoclay indicates the presence of mesoporous material with some blocked pores.

## 3.2. Modeling of black one acid removal process by modified montmorillonite

The present study explores the single and interactive effects of five process variables (initial dye concentration, pH, adsorbent dose, temperature, retention time) on the removal efficiency of AB1 dye. A total of 50 tests were conducted, and the results are outlined in Table 2.

Upon calculating the dye regression coefficient of AB1, the removal efficiency is modeled by the following equation, represented as equation (15):

$$\text{Removal} = 112.28 - 2.40A + 15.55B - 10.82C + 0.55D - 0.04E + 0.33AB + 0.04AC + 0.00018AD + 0.035AE - 0.18BC - 0.026BD - 0.23BE - 0.051CD + 0.10CE - 0.0079DE - 0.012A^2 - 1.39B^2 + 0.33C^2 - 0.005D^2 - 0.0046E^2 \quad (15)$$

The statistical significance and adequacy of the predicted model were analyzed using ANOVA and are presented in Table 3. The model F-value of 23.80 is significant, confirming the validity of the model. Furthermore, the very low probability value ($p >$ F-value less than 0.0001) indicates the significance of the model terms. The coefficient of variation (C.V.%) is less than 10, indicating sufficient accuracy. The signal-to-noise ratio, which is 19.84 in this study, surpasses the critical level of 4, further demonstrating the utility and capability of the model. In this model, parameters A, B, D, E, AB, AE, BE, CE, A2, B2, C2 were found to be significant ($P < 0.05$). The R2

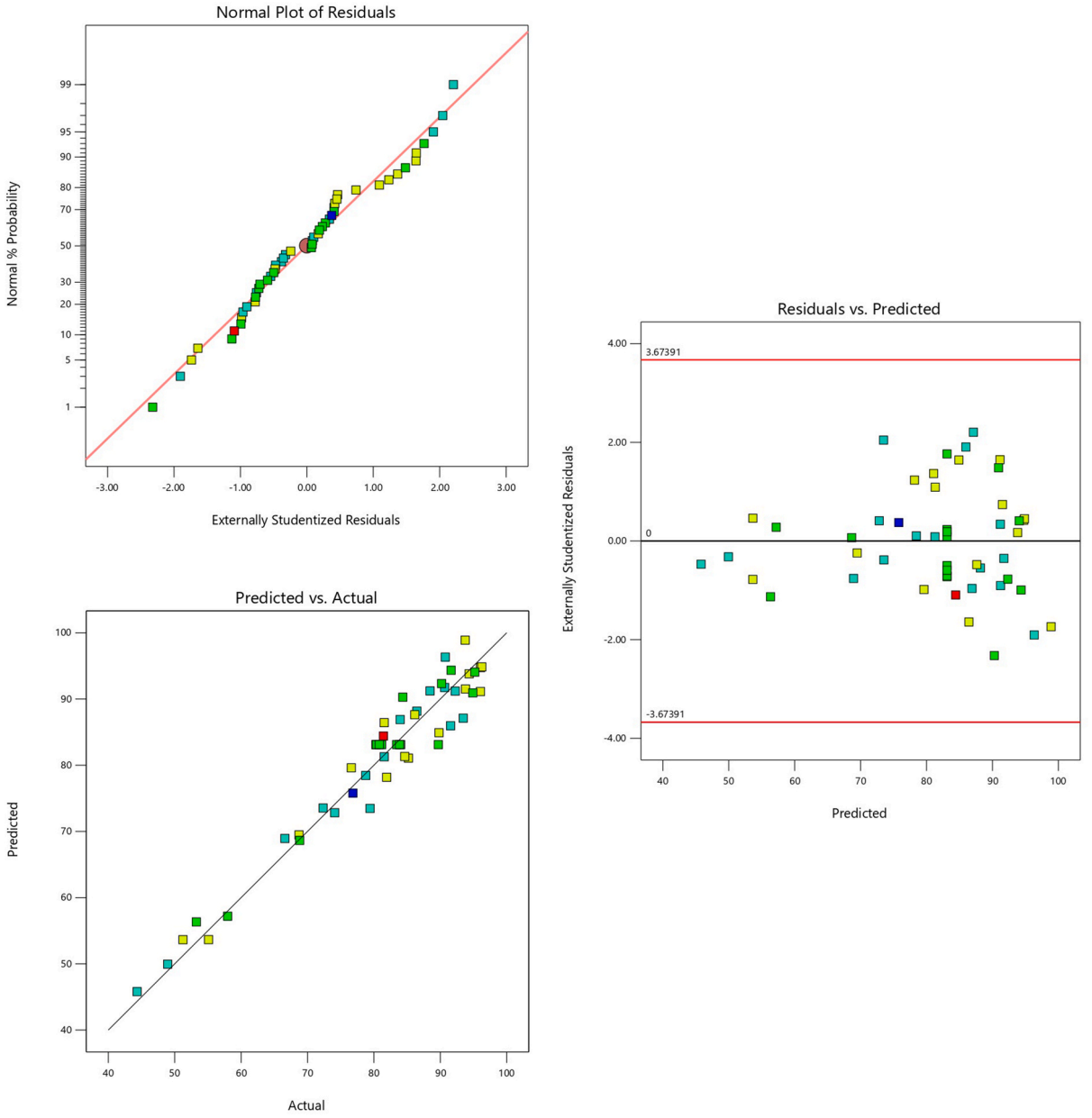


**Fig. 2.** a) Percentage of expected probability versus residual error b) Actual values versus predicted values c) Residual versus predicted response values in acid block removal.

value of the model is 0.9426, signifying that the model can explain approximately 95% of the total variation. The predicted R2 value (0.8079) demonstrates reasonable agreement with the adjusted R2 value (0.9030), supporting the high significance of all the expressions in the model. These statistical values demonstrate that the model is capable of accurately simulating the AB1 adsorption process.

The normal probability plot of raw residuals plays a crucial diagnostic tool for detecting systematic variance, assuming normal distribution and independence of errors, while their variance is linearly proportional to non-normality [42]. These characteristics validate the normal distribution of residuals, supporting the adequacy and applicability of the proposed model in explaining the experimental data. The plot of % normal probability against the normal plot of residuals exhibited a linear relationship, indicating the normal distribution of the data (Fig. 2a). A strong correlation was observed between the experimental values and the model-predicted removal efficiency values, as per equation (15) (Fig. 2b). The plot of % normal probability against the normal plot of residuals exhibited a linear relationship, indicating the normal distribution of the data (Fig. 2a). A strong correlation was observed between the experimental values and the model-predicted removal efficiency values, as per equation (15) (Fig. 2b). Additionally, the residual plot

**Table 2**
Actual and predicted values of black acid adsorption efficiency.

| Std | Run | A:Concentration | B: Dose | C: pH | D:Temperature | E: Time | Removal |
|---|---|---|---|---|---|---|---|
| 13 | 1 | 20 | 2 | 9 | 50 | 20 | 84.65 |
| 15 | 2 | 20 | 4 | 9 | 50 | 20 | 94.35 |
| 6 | 3 | 40 | 2 | 9 | 30 | 20 | 44.35 |
| 43 | 4 | 30 | 3 | 7 | 40 | 30 | 80.3 |
| 20 | 5 | 40 | 4 | 5 | 30 | 40 | 86.475 |
| 46 | 6 | 30 | 3 | 7 | 40 | 30 | 81.16 |
| 36 | 7 | 30 | 5.38 | 7 | 40 | 30 | 95.2 |
| 11 | 8 | 20 | 4 | 5 | 50 | 20 | 93.75 |
| 29 | 9 | 20 | 2 | 9 | 50 | 40 | 93.8 |
| 39 | 10 | 30 | 3 | 7 | 16.22 | 30 | 76.83 |
| 44 | 11 | 30 | 3 | 7 | 40 | 30 | 84.03 |
| 28 | 12 | 40 | 4 | 5 | 50 | 40 | 86.15 |
| 5 | 13 | 20 | 2 | 9 | 30 | 20 | 72.35 |
| 45 | 14 | 30 | 3 | 7 | 40 | 30 | 83.43 |
| 49 | 15 | 30 | 3 | 7 | 40 | 30 | 83.86 |
| 42 | 16 | 30 | 3 | 7 | 40 | 53.78 | 90.2 |
| 34 | 17 | 53.78 | 3 | 7 | 40 | 30 | 57.98 |
| 10 | 18 | 40 | 2 | 5 | 50 | 20 | 51.25 |
| 35 | 19 | 30 | 0.62 | 7 | 40 | 30 | 53.26 |
| 38 | 20 | 30 | 3 | 11.76 | 40 | 30 | 84.36 |
| 25 | 21 | 20 | 2 | 5 | 50 | 40 | 81.55 |
| 31 | 22 | 20 | 4 | 9 | 50 | 40 | 96.05 |
| 4 | 23 | 40 | 4 | 5 | 30 | 20 | 78.77 |
| 32 | 24 | 40 | 4 | 9 | 50 | 40 | 96.25 |
| 7 | 25 | 20 | 4 | 9 | 30 | 20 | 93.45 |
| 30 | 26 | 40 | 2 | 9 | 50 | 40 | 81.92 |
| 37 | 27 | 30 | 3 | 2.24 | 40 | 30 | 94.9 |
| 33 | 28 | 6.22 | 3 | 7 | 40 | 30 | 91.63 |
| 2 | 29 | 40 | 2 | 5 | 30 | 20 | 48.95 |
| 17 | 30 | 20 | 2 | 5 | 30 | 40 | 91.55 |
| 21 | 31 | 20 | 2 | 9 | 30 | 40 | 83.95 |
| 19 | 32 | 20 | 4 | 5 | 30 | 40 | 90.65 |
| 24 | 33 | 40 | 4 | 9 | 30 | 40 | 88.45 |
| 22 | 34 | 40 | 2 | 9 | 30 | 40 | 79.42 |
| 9 | 35 | 20 | 2 | 5 | 50 | 20 | 89.8 |
| 27 | 36 | 20 | 4 | 5 | 50 | 40 | 96.04 |
| 3 | 37 | 20 | 4 | 5 | 30 | 20 | 90.75 |
| 41 | 38 | 30 | 3 | 7 | 40 | 6.22 | 68.83 |
| 16 | 39 | 40 | 4 | 9 | 50 | 20 | 76.6 |
| 12 | 40 | 40 | 4 | 5 | 50 | 20 | 85.2 |
| 18 | 41 | 40 | 2 | 5 | 30 | 40 | 66.6 |
| 50 | 42 | 30 | 3 | 7 | 40 | 30 | 80.8 |
| 26 | 43 | 40 | 2 | 5 | 50 | 40 | 68.725 |
| 1 | 44 | 20 | 2 | 5 | 30 | 20 | 81.55 |
| 48 | 45 | 30 | 3 | 7 | 40 | 30 | 89.7 |
| 8 | 46 | 40 | 4 | 9 | 30 | 20 | 74.1 |
| 14 | 47 | 40 | 2 | 9 | 50 | 20 | 55.1 |
| 40 | 48 | 30 | 3 | 7 | 63.78 | 30 | 81.43 |
| 47 | 49 | 30 | 3 | 7 | 40 | 30 | 80.36 |
| 23 | 50 | 20 | 4 | 9 | 30 | 40 | 92.25 |

demonstrated a random scatter of residuals around the expected values (Fig. 2c), confirming a satisfactory fit of the model.

The response surface method (RSM) was employed to determine the most significant effects, considering all significant interactions between variables in the central composite design (CCD). Three-dimensional graphs (Fig. 3) illustrate how responses change with varying variables while keeping other variables at optimal values. The curvature of the graphs indicates the presence of interactions between variables. In Fig. 3, the interactive effect of adsorbent dose and the initial concentration of AB1 dye is depicted. The three-dimensional response surface plot illustrates high dye adsorption at a dose of 4 mg/30 mL and a concentration of 20 mg/L, attributed to the availability of a larger adsorption space due to a higher amount of adsorbent present. As the AB1 concentration decreases, the solute-to-vacant-adsorbent ratio increases, enhancing AB1 adsorption. Furthermore, with increasing contact time at low concentrations, a higher adsorption value is observed (Fig. 3). Conversely, adsorption increases with decreasing contact time and increasing adsorbent dose, as well as at high pH and contact time.

The optimal values indicated by RSM for pH, adsorbent mass, initial dye concentration, ultrasound time, and temperature were 5.46, 4 mg/30 mL, 20 mg/L, 20 min and 50 °C, respectively, with predicted adsorption of 96.49%. Subsequently, the adsorption was carried out in optimal conditions, achieving $92.83 \pm 1.19\%$, indicating a good match between the predicted and experimental data and confirming the adequacy of proposed model.

**Table 3**
Analysis of variance (ANOVA) for removal of AB1.

| Source | Sum of Squares | df | Mean Square | F-value | p-value | |
|---|---|---|---|---|---|---|
| **Model** | 8109.56 | 20 | 405.48 | 23.80 | <0.0001 | significant |
| A-concentration | 2640.95 | 1 | 2640.95 | 154.99 | <0.0001 | |
| B-Dose | 2724.46 | 1 | 2724.46 | 159.89 | <0.0001 | |
| C-pH | 0.7736 | 1 | 0.7736 | 0.0454 | 0.8328 | |
| D-Temprature | 142.31 | 1 | 142.31 | 8.35 | 0.0072 | |
| E-Time | 1074.04 | 1 | 1074.04 | 63.03 | <0.0001 | |
| AB | 361.74 | 1 | 361.74 | 21.23 | <0.0001 | |
| AC | 26.03 | 1 | 26.03 | 1.53 | 0.2264 | |
| AD | 0.0109 | 1 | 0.0109 | 0.0006 | 0.9800 | |
| AE | 409.55 | 1 | 409.55 | 24.04 | <0.0001 | |
| BC | 4.39 | 1 | 4.39 | 0.2575 | 0.6157 | |
| BD | 2.30 | 1 | 2.30 | 0.1350 | 0.7160 | |
| BE | 171.91 | 1 | 171.91 | 10.09 | 0.0035 | |
| CD | 34.51 | 1 | 34.51 | 2.03 | 0.1654 | |
| CE | 150.60 | 1 | 150.60 | 8.84 | 0.0059 | |
| DE | 19.99 | 1 | 19.99 | 1.17 | 0.2877 | |
| $A^2$ | 93.51 | 1 | 93.51 | 5.49 | 0.0262 | |
| $B^2$ | 108.74 | 1 | 108.74 | 6.38 | 0.0172 | |
| $C^2$ | 97.34 | 1 | 97.34 | 5.71 | 0.0236 | |
| $D^2$ | 15.77 | 1 | 15.77 | 0.9253 | 0.3440 | |
| $E^2$ | 12.00 | 1 | 12.00 | 0.7040 | 0.4083 | |
| **Residual** | 494.15 | 29 | 17.04 | | | |
| Lack of Fit | 424.81 | 22 | 19.31 | 1.95 | 0.1851 | not significant |
| Pure Error | 69.34 | 7 | 9.91 | | | |
| **Cor Total** | 8603.72 | 49 | | | | |

### *3.2.1. Adsorption equilibrium study*

The adsorption isotherm delineates the distribution of adsorbate molecules between the adsorbent and the liquid phase at equilibrium, as a function of the adsorbent concentration. This investigation utilized the equilibrium adsorption isotherm models of Langmuir, Freundlich, and Temkin under optimal conditions, as depicted in Fig. 4 a-c. By comparing the coefficient of determination (R2) values derived from these models, we determined the most suitable model. The specific parameters acquired from curve fitting are documented in Table 4. The findings derived from this study suggest that the Freundlich isotherm offers the most precise depiction of the adsorption behavior of AB1 on the modified montmorillonite within the stipulated experimental parameters. This assertion is supported by the superior R2 value achieved by the Freundlich isotherm in comparison with the Langmuir and Temkin models, demonstrating its superior fit to the observed data. The Freundlich model, distinguished by its capacity for multilayer adsorption, intimates that the process under investigation is underpinned by a comparable multilayer adsorption mechanism [43]. Additionally, the substantial maximum adsorption capacity, specifically quantified at 120.48 mg/g, signifies the impressive potential of the adsorbent in removing AB1. The RL value, which lies between 0 and 1 (precisely 0.15), as derived from the Langmuir model, further corroborates the feasibility and reversibility of the adsorption process. Nevertheless, the Freundlich model's obtained n values are less than 1, deviating from the commonly reported range of 1–10 in numerous studies. These values are indicative of a weak interaction between the adsorbent and adsorbate or a concentration-dependent adsorption process. While this opens up an avenue for potential performance enhancement, the overall evaluation distinctly underlines the efficacy of the scrutinized adsorbent in the removal of AB1.

In the detailed analysis of the kinetic adsorption data for the AB1 dye, we employed three unique models: the intraparticle diffusion model, the pseudo-first-order kinetic model, and the pseudo-second-order kinetic model. These models are visually represented in Fig. 5 a-c. The results of these calculations have been systematically tabulated in Table 4. Of particular note is the outstanding alignment of the pseudo-second-order kinetic model with the experimental data, as demonstrated by a near-perfect correlation coefficient of 0.9999. This suggests that the pseudo-second-order model provides an extraordinarily accurate depiction of the kinetic dynamics of the process.

Furthermore, these data substantiate the premise that chemisorption, characterized by site-specific electrostatic interaction, serves as the rate-determining step in the adsorption of AB1 onto octadecylamine-functionalized nanoclay. This chemisorption implies a strong bond between the adsorbate and the adsorbent, indicative of a chemical linkage [44]. The primary conclusion drawn from this study emphasizes the essential role of chemisorption in the kinetic behavior of AB1 adsorption onto the functionalized nanoclay.

Thermodynamic considerations are crucial for assessing the spontaneity of an adsorption process. The adsorption coefficient in chemical reactions is known to be influenced by changes in ambient temperature. To explore this effect, dye adsorption experiments were conducted within a temperature range of 20–60 °C. The experimental data obtained at different temperatures were utilized to calculate thermodynamic parameters, including Gibbs free energy change ($\Delta G^\circ$), enthalpy change ($\Delta H^\circ$), and entropy change ($\Delta S^\circ$) °), as depicted in Fig. 6. The resulting thermodynamic parameters for the adsorption of AB1 on modified montmorillonite are presented in Table 4 The determination of $\Delta H^\circ$ and $\Delta S^\circ$ involved analyzing the slope and intercept of the ln KD versus 1/T plot.

The positive $\Delta H^\circ$ value (26.41 kJ/mol) suggests that the adsorption of AB1 on modified montmorillonite is an endothermic reaction. The calculated $\Delta G^\circ$ value confirms the spontaneous nature of the adsorption process. Additionally, the positive $\Delta S^\circ$ value (123.58 J/mol K), indicates the affinity of modified montmorillonite towards AB1 dye. Additionally, the positive $\Delta S^\circ$ value (123.58 J/

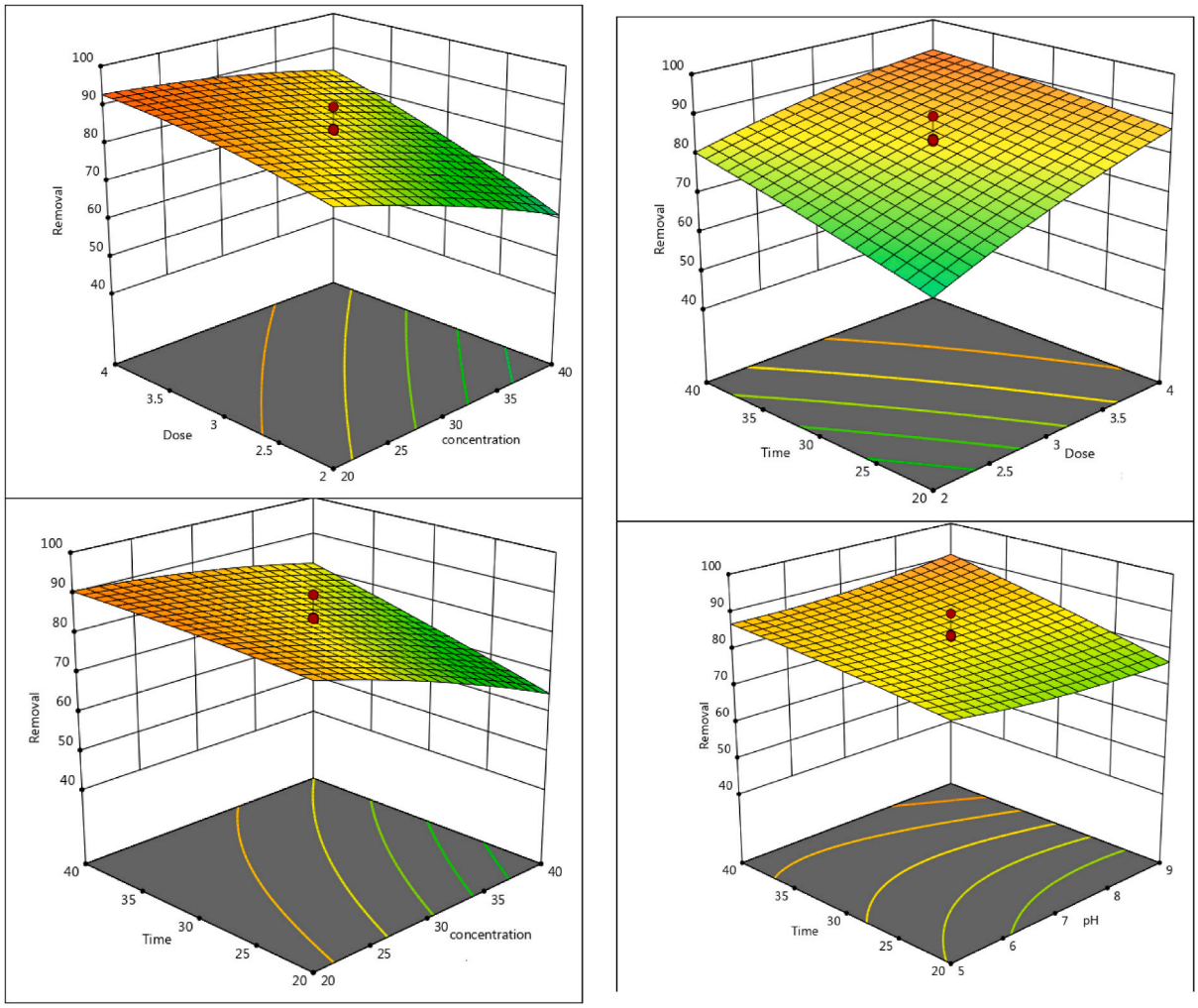


**Fig. 3.** The 3D interaction effect of significant parameters in the AB 1 removal.

mol K) suggests the affinity of modified montmorillonite towards AB1 dye. Notably, as the temperature rises from 293 to 333 K, dye adsorption significantly increases. This enhancement in the adsorption capacity of modified montmorillonite can be attributed to the enlargement of pore size and activation of the adsorbent surface with temperature. Furthermore, higher temperatures enhance the mobility of large dye ions while reducing the swelling effect, facilitating deeper penetration of the large dye molecules. The results also reaffirm that the adsorption of AB1 is an endothermic process.

The efficacy of the introduced method has undergone rigorous assessment and comparisonwith alternative techniques and diverse adsorbents. An exhaustive comparison is encapsulated inTable 5, highlighting the enhanced adsorption capability of the suggested method. Thefabrication procedure of the recommended adsorbent is distinctly more streamlined compared tomany specimens enumerated in table. By leveraging natural Montmorillonite as afoundational material, our adsorbent not only facilitates straightforward synthesis but also26promotes a diminished ecological impact. Furthermore, as substantiated by the data in Table 5,our adsorbent manifests a preeminent adsorption capability for specific pollutants, notably blackacid 1. In conclusion, while some adsorbents may exhibit an elevated maximum adsorptioncapacity, the confluence of synthesis efficiency, environmental sustainability, and robustperformance positions our adsorbent as a compelling contender for black acid 1 remediation.

## 4. Conclusion

The research showcased the effectiveness of montmorillonite as an adsorbent for AB1 removal. The study systematically investigated the impact of various experimental parameters, including initial concentration, contact time, pH, adsorbent dose, and temperature on the percentage of AB1 removal. Employing an experimental design in an aqueous solution, we optimized conditions for AB1 removal using montmorillonite modified with octadecylamine and ultrasound. The study revealed that an increase in adsorbent dose, temperature, and contact time significantly accelerated dye removal. By optimizing pH (5.46), adsorbent mass (4 mg/30 mL),

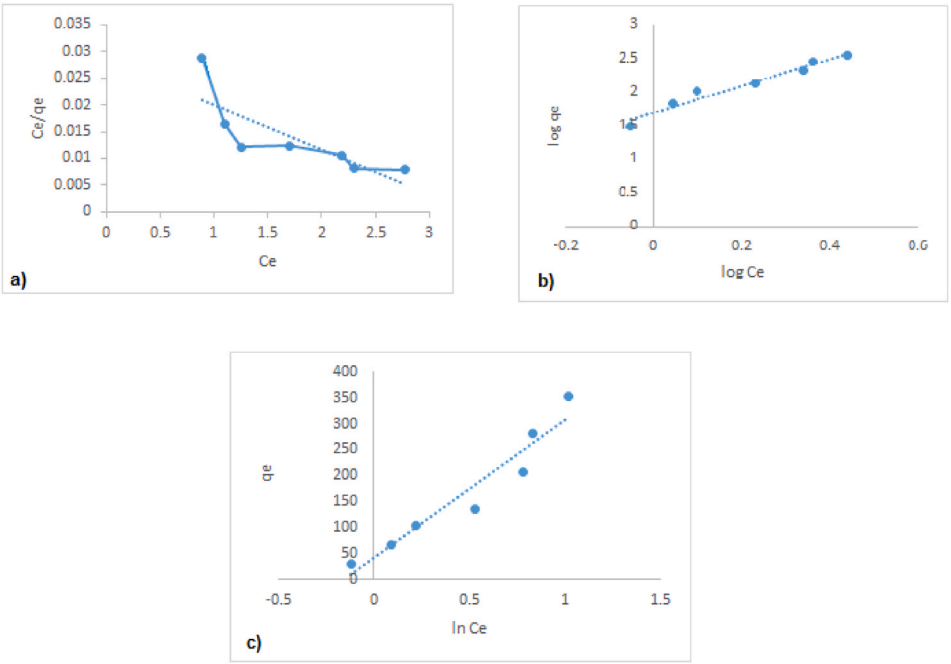


**Fig. 4.** The adsorption isotherms of AB1 in nanoclay a) Langmuir b) Freundlich c) Temkin.

**Table 4**
Parameters of kinetic and isothermal models for MB adsorption by the synthesized magnetite nanoparticle.

| | Model | Parameters | Value |
|---|---|---|---|
| Kinetic models | Pseudo-first-order (PFO) | $q_e$ (mg $g^{-1}$) | 19.92 |
| | | $k_1(min)^{-1}$ | 0.1348 |
| | | $R^2$ | 0.8318 |
| | Pseudo-second-order (PSO) | $q_e$ (mg $g^{-1}$) | 140.85 |
| | | $k_2$ (g $mg^{-1}$ $min^{-1}$) | 0.0263 |
| | | $R^2$ | 0.9999 |
| | Intraparticle diffusion | K | 6.12 |
| | | C | 111.83 |
| | | $R^2$ | 0.7936 |
| Isothermal models | Langmuir | $q_m$ | 120.48 |
| | | b | 0.29 |
| | | $R^2$ | 0.638 |
| | Freundlich | $K_F$ | 49.93 |
| | | $\frac{1}{n}$ | 1.98 |
| | | $R^2$ | 0.9589 |
| | Temkin | $K_T$ | 1.16 |
| | | b | 10.03 |
| | | $R^2$ | 0.9254 |

| | T (K) | 293 | 303 | 313 | 323 | 333 |
|---|---|---|---|---|---|---|
| Adsorption thermodynamics | ΔG (kJ/mol) | −9.84 | −10.90 | −12.34 | −13.58 | −14.68 |
| | ΔH (kJ/mol) | | | 26.41 | | |
| | ΔS (kJ/mol.K) | | | 123.58 | | |
| | $R^2$ | | | 0.9953 | | |

initial dye concentration (20 mg/L), ultrasound time (20 min), and temperature (50 °C), we achieved an impressive adsorption rate of 96.49%. Equilibrium, kinetic, and thermodynamic studies further enriched our understanding. The Freundlich model emerged as the most suitable for describing the equilibrium data, while the pseudo-second-order kinetic model successfully represented the kinetics of the process. Thermodynamic analysis confirmed AB1 adsorption as an endothermic process.

In summary, these findings highlight the potential of montmorillonite modified with octadecylamine as an effective adsorbent for removal of anionic dye from aqueous solutions.

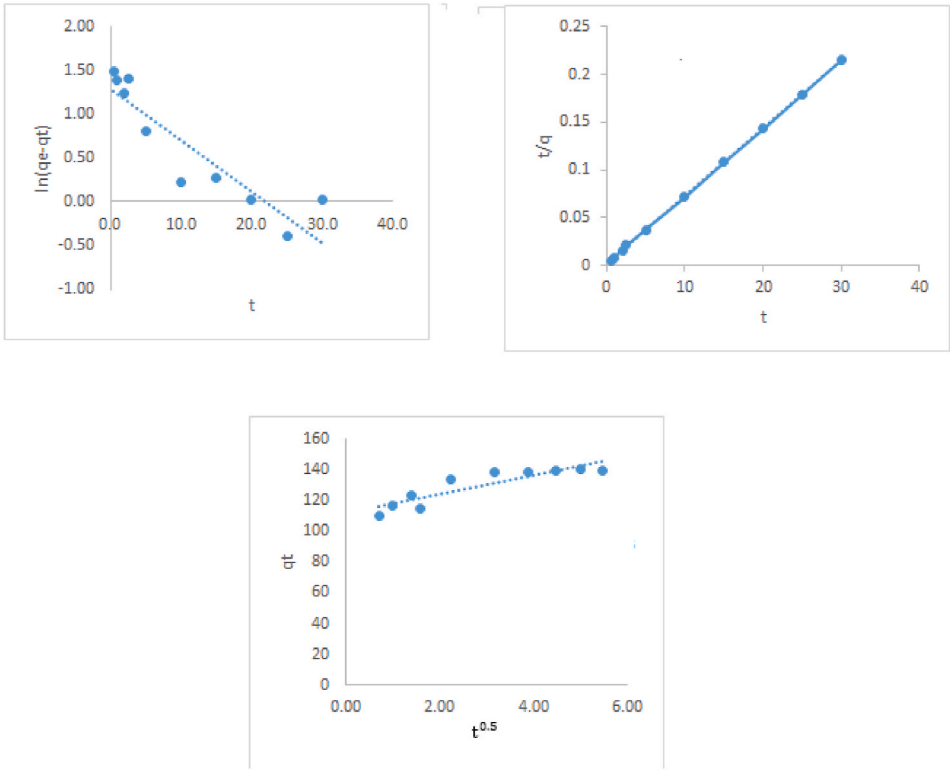


**Fig. 5.** Kinetic models for the adsorption of AB1: (a) pseudo-first-order (b) pseudo-second-order (c) intraparticle diffusion.

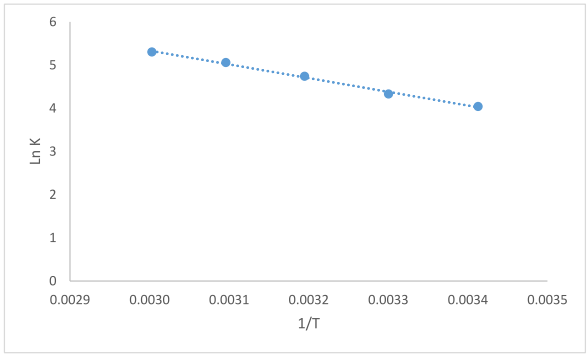


**Fig. 6.** Enthalpy and entropy determination for AB1 removal.

**Table 5**
Comparison of Black Acid 1 adsorption on different adsorbents.

| No. | Adsorbent | $q_{max}$(mg/g) | Ref. |
|---|---|---|---|
| **1** | **Pine-cone derived activated carbon** | **452.9** | [45] |
| **2** | **Chromium-tanned leather waste** | **980.4** | [46] |
| **1** | **His-MNPs** | **166.7** | [47] |
| **3** | **potato peel waste biomass** | **1.79** | [48] |
| **5** | **Amine-Functionalized Carbon Nanotubes** | **714** | [49] |
| **6** | **cationic hydrogel adsorbent** | **1771** | [50] |
| **This study** | **octadecylamine loaded on montmorilonite** | **120.48** | - |

## Funding

This research was supported by Shiraz University of Medical Sciences (Grant number 23971).

## Ethical approval

Not applicable.

## Consent to participate

The authors declare their Consent to Participate in this article.

## Consent to publish

The authors declare their Consent to Publish this article.

## Availability of data and materials

Data will be made available on request.

## CRediT authorship contribution statement

**Fatemeh Keshavarzi:** Writing – original draft. **Mohammad Reza Samaei:** Writing – review & editing, Project administration, Investigation, Conceptualization. **Hassan Hashemi:** Writing – review & editing, Conceptualization. **Abooalfazl Azhdarpoor:** Writing – review & editing, Validation. **Amin Mohammadpour:** Writing – review & editing, Formal analysis.

## Declaration of generative AI and AI-assisted technologies in the writing process

We leveraged artificial intelligence to enhance the quality of the manuscript.

## Declaration of competing interest

The authors declare that they have no known competing financial interests or personal relationships that could have appeared to influence the work reported in this paper.

## References

[1] M. Dehghani, et al., Determination of chloroform concentration and human exposure assessment in the swimming pool, Environ. Res. 203 (2022) 111883.
[2] F. Abbasi, et al., Removal, optimization and kinetic modeling of high concentration of methyl tertiary butyl ether from aqueous solutions using copper oxide nanoparticles and hydrogen peroxide, Desalination and Water Treat. 181 (2020) 278–288.
[3] A. Mohammadpour, et al., Concentration, distribution and probabilistic health risk assessment of exposure to fluoride in drinking water of Hormozgan province, Iran, Stoch. Environ. Res. Risk Assess. (2022) 1–13.
[4] T. Shindhal, et al., A critical review on advances in the practices and perspectives for the treatment of dye industry wastewater, Bioengineered 12 (1) (2021) 70–87.
[5] N. Karami, et al., Green synthesis of sustainable magnetic nanoparticles Fe3O4 and Fe3O4-chitosan derived from Prosopis farcta biomass extract and their performance in the sorption of lead(II), Int. J. Biol. Macromol. 254 (2024) 127663.
[6] S. Mani, R.N. Bharagava, Exposure to crystal violet, its toxic, genotoxic and carcinogenic effects on environment and its degradation and detoxification for environmental safety, Rev. Environ. Contam. Toxicol. 237 (2016) 71–104.
[7] L. Mohammadi, et al., Optimization of photocatalytic degradation of biochemical oxygen demand from textile industry effluent using copper oxide nanoparticles by response surface methodology, Environ. Prog. Sustain. Energy 42 (1) (2023) e13962.
[8] D. Bhatia, et al., Biological methods for textile dye removal from wastewater: a review, Crit. Rev. Environ. Sci. Technol. 47 (19) (2017) 1836–1876.
[9] S. Samsami, et al., Recent advances in the treatment of dye-containing wastewater from textile industries: overview and perspectives, Process Saf. Environ. Protect. 143 (2020) 138–163.
[10] S. El Harfi, A. El Harfi, Classifications, properties and applications of textile dyes: a review, Appl. J. Environ. Eng.Sci. 3 (3) (2017) 00000-3. N° 3 (2017) 311-320.
[11] L. Nambela, L.V. Haule, Q. Mgani, A review on source, chemistry, green synthesis and application of textile colorants, J. Clean. Prod. 246 (2020) 119036.
[12] A.B. Rostam, M. Taghizadeh, Advanced oxidation processes integrated by membrane reactors and bioreactors for various wastewater treatments: a critical review, J. Environ. Chem. Eng. 8 (6) (2020) 104566.
[13] A. Chaturvedi, et al., A comprehensive review on the integration of advanced oxidation processes with biodegradation for the treatment of textile wastewater containing azo dyes, Rev. Chem. Eng. 38 (6) (2021) 1–18.
[14] L. Mohammadi, et al., Removal of amoxicillin from aqueous media by fenton-like sonolysis/H2O2 process using zero-valent iron nanoparticles, Molecules 27 (19) (2022) 6308.
[15] R. Ashoori, et al., Simultaneous removal of fluoride and nitrate from synthetic aqueous solution and groundwater by the electrochemical process using non-coated and coated anode electrodes: a human health risk study, Environ. Res. 214 (2022) 113938.
[16] L. Natrayan, et al., Synthesis and analysis of impregnation on activated carbon in multiwalled carbon nanotube for Cu adsorption from wastewater, Bioinorgan. Chem. Appl. 2022 (2022).
[17] K.M. Chahrour, et al., CuO/Cu/rGO nanocomposite anodic titania nanotubes for boosted non-enzymatic glucose biosensors, New J. Chem. 47 (16) (2023) 7890–7902.

[18] A. Gautam, et al., Colloidal synthesis of a heterostructured CuCo 2 S 4/gC 3 N 4/In 2 S 3 nanocomposite for photocatalytic hydrogen evolution, Energy Adv. 2 (9) (2023) 1512–1520.
[19] M.S. Iqbal, et al., The potential of functionalized graphene-based composites for removing heavy metals and organic pollutants, J. Water Proc. Eng. 53 (2023) 103809.
[20] M. Ahmadipour, et al., Photodegradation of rhodamine B-dye pollutant using CaCu3Ti4O12-multiwall carbon nanotube nanocomposites, J. Environ. Chem. Eng. 9 (3) (2021) 105185.
[21] H. He, et al., Preparation of MOFs and MOFs derived materials and their catalytic application in air pollution: a review, Catal. Today 375 (2021) 10–29.
[22] A. Jayakumar, et al., Recent innovations in bionanocomposites-based food packaging films–A comprehensive review, Food Packag. Shelf Life 33 (2022) 100877.
[23] N. Khatoon, M.Q. Chu, C.H. Zhou, Nanoclay-based drug delivery systems and their therapeutic potentials, J. Mater. Chem. B 8 (33) (2020) 7335–7351.
[24] I. Derungs, et al., Influence of the hydrophilicity of montmorillonite on structure and properties of thermoplastic wheat starch/montmorillonite bionanocomposites, Polym. Adv. Technol. 32 (11) (2021) 4479–4489.
[25] C.H. Tay, et al., Mechanical performance of hybrid glass/kenaf epoxy composite filled with organomodified nanoclay, J. Mater. Res. Technol. 15 (2021) 4415–4426.
[26] C. Zhao, et al., Octadecylamine and serine-derived carbon dots-modified silica gel for reversed phase/hydrophilic interaction liquid chromatography, Microchem. J. 183 (2022) 107987.
[27] S. Benkhaya, S. M'Rabet, A. El Harfi, Classifications, properties, recent synthesis and applications of azo dyes, Heliyon 6 (1) (2020) e03271.
[28] K.-W. Jung, et al., Aluminum carboxylate-based metal organic frameworks for effective adsorption of anionic azo dyes from aqueous media, J. Ind. Eng. Chem. 59 (2018) 149–159.
[29] R. Al-Tohamy, et al., A critical review on the treatment of dye-containing wastewater: ecotoxicological and health concerns of textile dyes and possible remediation approaches for environmental safety, Ecotoxicol. Environ. Saf. 231 (2022) 113160.
[30] F. Yang, et al., Kinetics and mechanism analysis of CO2 adsorption on LiX@ZIF-8 with core shell structure, Powder Technol. 399 (2022) 117090.
[31] A. Pandiarajan, et al., OPAC (orange peel activated carbon) derived from waste orange peel for the adsorption of chlorophenoxyacetic acid herbicides from water: adsorption isotherm, kinetic modelling and thermodynamic studies, Bioresour. Technol. 261 (2018) 329–341.
[32] M. Ahmadipour, M.F. Ain, Z.A. Ahmad, A short review on copper calcium titanate (CCTO) electroceramic: synthesis, dielectric properties, film deposition, and sensing application, Nano-Micro Lett. 8 (4) (2016) 291–311.
[33] W. Sajjad, et al., Development of modified montmorillonite-bacterial cellulose nanocomposites as a novel substitute for burn skin and tissue regeneration, Carbohydr. Polym. 206 (2019) 548–556.
[34] A. Abdel-Karim, et al., High-performance mixed-matrix membranes enabled by organically/inorganic modified montmorillonite for the treatment of hazardous textile wastewater, Chem. Eng. J. 405 (2021) 126964.
[35] D.A. Almasri, et al., High performance hydroxyiron modified montmorillonite nanoclay adsorbent for arsenite removal, Chem. Eng. J. 335 (2018) 1–12.
[36] G. Damian, et al., Mineralogical and physico-chemical characterization of the oraşu-nou (Romania) bentonite Resources, Minerals 11 (2021), https://doi.org/10.3390/min11090938.
[37] M. Ahmadipour, et al., Assessment of crystallite size and strain of CaCu3Ti4O12 prepared via conventional solid-state reaction, Micro & Nano Lett. 11 (3) (2016) 147–150.
[38] S.T. Olalekan, et al., Effect of modification on the physicochemical and thermal properties of organophilic clay modified with octadecylamine, Int. J. Eng. Technol. 10 (1) (2010) 27–35.
[39] A.K. Barick, D.K. Tripathy, Effect of organoclay on the morphology, mechanical, thermal, and rheological properties of organophilic montmorillonite nanoclay based thermoplastic polyurethane nanocomposites prepared by melt blending, Polym. Eng. Sci. 50 (3) (2010) 484–498.
[40] Y. Ma, et al., Infrared investigation of organo-montmorillonites prepared from different surfactants, Spectrochim. Acta Mol. Biomol. Spectrosc. 76 (2) (2010) 122–129.
[41] S. Labidi, et al., Organo-modified montmorillonite/poly (ε-caprolactone) nanocomposites prepared by melt intercalation in a twin-screw extruder, Polym. Degrad. Stabil. 95 (3) (2010) 382–388.
[42] A. Singh, A. Yadav, N.R. Bishnoi, Statistical screening and optimization of process variables for xylanase production utilizing alkali-pretreated rice husk, Ann. Microbiol. 63 (1) (2013) 353–361.
[43] S.M. Pormazar, A. Dalvand, Adsorption of Direct Red 23 dye from aqueous solution by means of modified montmorillonite nanoclay as a superadsorbent: mechanism, kinetic and isotherm studies, Kor. J. Chem. Eng. 37 (2020) 2192–2201.
[44] M. Mehdizadeh, et al., The Effect of Arsenic on the Photocatalytic Removal of Methyl Tet Butyl Ether (MTBE) Using $Fe_2O_3$/MgO Catalyst, Modeling, and Process Optimization, Catalysts 12 (2022) 927.
[45] M. Hadi, M.R. Samarghandi, G.J.C.E.J. McKay, Equilibrium two-parameter isotherms of acid dyes sorption by activated carbons: study of residual errors 160 (2) (2010) 408–416.
[46] X. Peng, et al., Adsorption removal of acid black 1 from aqueous solution using ordered mesoporous carbon 294 (2014) 71–80.
[47] A. Qurrat ul, et al., Convenient pH-responsive removal of Acid Black 1 by green l-histidine/iron oxide magnetic nanoadsorbent from water: performance and mechanistic studies, RSC Adv. 9 (6) (2019) 2978–2996.
[48] E. Hoseinzadeh, et al., Removal of acid dyes from aqueous solution using potato peel waste biomass: a kinetic and equilibrium study, Desalination Water Treat. 52 (25–27) (2014) 4999–5006.
[49] U. Hamesadeghi, et al., Adsorption of Acid Black 1 dye from aqueous solution by amine-functionalized carbon nanotubes, J. Health 7 (2016) 643–655.
[50] R. Fang, et al., Synthesis and characterization of a high-capacity cationic hydrogel adsorbent and its application in the removal of Acid Black 1 from aqueous solution, React. Funct. Polym. 102 (2016) 1–10.